Hindawi
Mathematical Problems in Engineering
Volume 2018, Article ID 1329187, 13 pages
https://doi.org/10.1155/2018/1329187

Research Article

Numerical Investigation of Particle Concentration Distribution Characteristics in Twin-Tunnel Complementary Ventilation System

Rui Ren,[1] **Shuoshuo Xu**,[1] **Zhaodan Ren**,[2] **Shuangzhuo Zhang**,[2] **Hao Wang**,[3] **Xiuling Wang**,[1] **and Siyue He**[1]

[1]*School of Highway, Chang'an University, Xi'an 710064, China*
[2]*China Railway Siyuan Survey and Design Group Co., Ltd, Wu'han 430063, China*
[3]*School of Civil & Construction Engineering, Oregon State University, 101 Kearney Hall, Corvallis, OR 97331, USA*

Correspondence should be addressed to Xiuling Wang; wangxiuling@chd.edu.cn

Received 6 January 2018; Revised 2 June 2018; Accepted 20 June 2018; Published 12 July 2018

Academic Editor: Babak Shotorban

Longitudinal ventilation systems are commonly installed in new tunnels. In this paper, based on the similarity law, the scale model with a view to different conditions is carried out to study the effectiveness of twin-tunnel complementary ventilation system. The system can offer enough amount of fresh air to meet requirement of driving safety by using longitudinal ventilation without ventilation shaft. Field measurements were also performed to validate the numerical model. Results reveal that particle concentration distribution is influenced by the distance from air interchange cross-passages to uphill tunnel inlet (L_{ex}) and the flow volume of air interchange cross (Q_{ex}) passage and jet fan thrust (P_{jet}) in tunnel. And L_{ex} is the most important factor about influencing the ventilation efficiency.

1. Introduction

To provide sufficient fresh air and dilute toxic gases from vehicles, mechanical ventilation systems with jet fans or shafts are often employed [1, 2]; however ventilation shafts need high energy consumption ventilation equipment such as jet fans. This paper introduced a relatively novel ventilation system, namely, twin-tunnel complementary ventilation system. The system has two-air interchange cross-passages between uphill tunnel and downhill tunnel which can meet the requirement of fresh air in tunnel. Compared with traditional ventilation system, the twin-tunnel complementary ventilation system is a relatively innovative method, which has a number of advantages including low consumption of energy and construction, multiplexing, more reasonable distribution of pollutant concentration, and good visibility.

Ventilation of resident buildings plays an important role in providing better indoor air quality (IAQ) and thermal comfort [3–7]. Many simulations and field tests have been conducted about building ventilation [8, 9]. In recent years, the construction of tunnels has developed rapidly in China [10–20] and a lot of difficult problems have been solved [21–30]. Ventilation of tunnels plays an important role in reducing the emission of toxic gas, maintaining good visibility, and controlling the fire in tunnels [31–33]. The mechanical ventilation can be performed with three approaches: longitudinal, transverse [34, 35], semitransverse [36, 37]. Among these ventilation systems, longitudinal ventilation system equipped with jet fans has been most widely adopted owing to effective utilization of the piston wind [38]. In the last decades, many scholars have done much research on the mechanical ventilation system of long tunnels. Bogdan. S et al. [39] proved that appropriate number of jet fans is the important factor to reach desirable air quality in longitudinal ventilation system. Wang et al. [40, 41] investigated the aerodynamic behavior of jet fans in a curved road tunnel and its effects of deflected angles of jet fans on the tunnel ventilation system. The pollution concentration increases along the tunnel in the airflow direction with

longitudinal ventilation system. In order to increase the need for effective ventilation for removing toxic gases emitted by vehicles from the tunnels especially during traffic jams, Bari et al. [42] studied the ventilation effectiveness of the Banana jet fan. Comparing the performance of longitudinal ventilation systems for road tunnel equipped with alternative jet fans and traditional jet fans in case of fire, Musto and Rotondo [43] presented the results that longitudinal ventilation system equipped with alternative jet fan require lower total thrust with respect to traditional jet fans to prevent back-layering. Kazemipour, Afshin, and Farhanieh [44] investigated the influence of longitudinal jet fan location relative to fire and its vertical position. They showed that the jet fan performance degraded because jet fan air flow spread would attack the rising smoke plume and lead to dynamic losses; then its actual thrust increased with lowering the jet fan installation height. Lee, Ryou [45], and Tang et al. [46, 47] performed the influence of smoke movement in a longitudinal ventilated tunnel fires. In short tunnels, the nature ventilation and the piston effect of moving vehicles are usually sufficient to drive fresh air in and discharge polluted air out [48, 49]. However, in long vehicle tunnels, the mechanical ventilation system is required to dilute toxic gases emitted by vehicles [50–53]. And because of the topographic constraint, in some large single-slope double-line tunnels, the particle emissions in uphill tunnel are larger than in downhill tunnel. If the longitudinal ventilation with jet fans is adopted in the single-slope twin-tunnels, the airflow requirements cannot be fulfilled due to high wind speeds in the uphill tunnel and only smaller amounts of air are needed in downhill tunnel to ensure air quality and visibility thresholds. Traditionally, a shaft or inclined shaft is used as the ventilation in tunnels for air exchange [54–57], which bring about increase of ventilation system initial investment and operation energy consumption. To solve the imbalance of ventilation requirement between uphill tunnel and downhill tunnel, Bemer and Day (1991) [58] proposed the concept of "twin-tunnel complementary" ventilation for the first time, which considers the tunnel as a single unit rather than as two separated tunnels. The concept came into practice for the first time in Ping-Lin tunnel in Taiwan, and the investment and operation cost of the tunnel reduced largely [59]. From then on, several studies have been performed in order to better understand the system [60–65].

In this paper, CFD simulations were conducted under different conditions (AIAA, 1998) [66]. More specifically, experimental measurement was carried out to validate the results of a three-dimensional numerical model. The aim of study is to reveal the distribution of pollution concentration in twin-tunnel complementary ventilation system. The results can help engineers to better understand the effect on the pollution concentration adjustment between uphill tunnel and downhill tunnel, to design an effective ventilation system for double-line tunnel.

2. Complementary Ventilation System

2.1. Engineering Overview. A substantial number of tunnel projects have been constructed in complex geological area as western development strategies have been implemented

Figure 1: Dabieshan Tunnel.

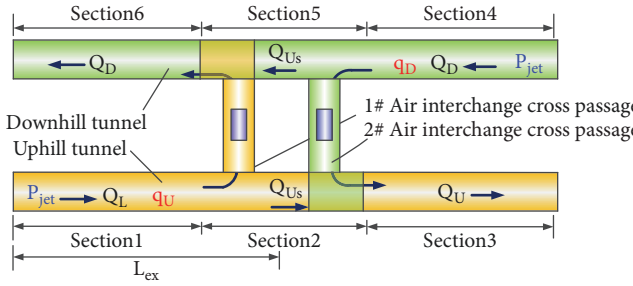

Figure 2: Twin-tunnel complementary ventilation system.

in China [25, 67–71]. The purpose of the present study is to understand the effect of the twin-tunnel complementary ventilation system on the distribution of pollutants in Dabieshan tunnel which is one of the main highway tunnels linking Wuhan with Macheng. The tunnel consists of two separated tunnels with large single-slope whose direction is one-way. The uphill tunnel is 4910 m with slope of 4% and the downhill tunnel is 4908 m with slope of -4%, show in Figure 1. The tunnel cross-section is 62.8 m^2 and the maximum width and the height of the tunnel cross-section are 11.2 m and 7.5 m, respectively. When the vehicle speed reaches 50km/h, the requirement for fresh air volume of the uphill tunnel (Q_{Ureq}) and downhill tunnel (Q_{Dreq}) is 460m^3/s and 95m^3/s respectively, and the air velocity of V_{Ureq} and V_{Dreq} is 7.35m/s and 1.5m/s, respectively. Due to high wind speeds in the uphill tunnel, airflow requirements cannot be fulfilled, so the tunnel needs a shaft or inclined shaft in the uphill tunnel for air exchange. However, the average airflow requirements Q_{aver} of uphill tunnel and downhill tunnel is only 277.5m^3/s and the average air velocity V_r of the twin-tunnel is only 4.42 m/s, and then the twin-tunnel complementary ventilation system was employed.

The twin-tunnel complementary ventilation system has two-air interchange cross-passages to connect the two tunnels, which divide the tunnels into 6 sections, and the distance between two-air interchange cross-passages is 100m, far less than the length of tunnel. Section 1, section 2, and section 3 are in uphill tunnel and section 4, section 5, and section 6 are in downhill tunnel, as shown in Figure 2. The high concentrated polluted air in section 1 passes through 1# air interchange cross-passage into section 6, a part of the pollutants in section 1 will be transferred to section 6, and

the total amount of transferred pollutants is q_{ex1}. Combing with transferred pollutants, the pollutions in section 6 discharges through the downhill tunnel outlet, and the particle concentration of downhill tunnel is C_D. The low concentrate polluted air in section 4 through the 2# air interchange cross-passage into the section 3, a part of the pollutants in section 4 will be transferred to the section 3, and the total amount of transferred pollutants is q_{ex2}. Combing with transferred pollutants, the pollutions in section 3 discharges through the uphill tunnel outlet, and the particle concentration of uphill tunnel outlet is C_U. The particle concentration ratio of uphill tunnel and downhill tunnel C_U/C_D is index, which is used to evaluate the efficiency of adjusting the particle concentration distribute in uphill tunnel and downhill tunnel by twin-tunnel complementary ventilation. When $C_U/C_D = 1$, the efficiency of adjusting achieves the best result, and when the $C_U/C_D > 1$, the adjusting is excessed.

Where Q_U and Q_D are the fresh air requirement volume in the uphill tunnel and the downhill tunnel, respectively, q_U and q_D are the amount of particle emission from the cars in the uphill tunnel and the downhill tunnel, respectively, L_{ex} is the distance from the air interchange cross-passages to uphill tunnel inlet, Q_{ex} is the flow volume of air interchange cross-passage, P_{jet} is jet fan thrust in tunnel, and L is the length of tunnel.

2.2. Methodology. Field measurement was carried out to reveal the characteristics of air flow and particle concentration distribution in the twin-tunnels with twin-tunnel complementary ventilation system. There are a total of eight cross-sections to be tested as shown in Figure 3. A hot wire anemometer which has a resolution of 0.01 m/s was employed to test the air velocity, and Light transmittance instrument which has resolution of 0.0001/m was used to measure the particle concentration by testing the extinction coefficient in 100 m range. Testing preparation and testing process is shown in Figure 4. The cross-section of the base tunnel (cross-sections I-I, II-II, III-III, IV-IV, V-V, and VI-VI) is divided into fourteen parts and the cross-section of the cross-passage (cross-sections VII-VII and VIII-VIII) is divided into nine parts, as shown in Figure 3. The air velocity and particle concentration at the centroid of each part were recorded for 10min at 1min intervals. All the air velocity and particle concentration records of each part were averaged to v_i and C_i separately. Hence, the average air velocity v_{av} and particle concentration C_{av} of the cross-section can be calculated as (1)~(2):

$$v_{av} = \frac{\sum a_i v_i}{\sum a_i} \tag{1}$$

$$C_{av} = \frac{\sum a_i C_i}{\sum a_i} \tag{2}$$

where (1) $i = 1, \ldots, 14$ for base tunnel and (2) $i = 1, \ldots, 9$ for cross-passage and a_i is the area of part i in the cross-section.

3. Numerical Methodology

3.1. Governing Equations. The computational fluid dynamics (CFD) software ANSYS Fluent (15.0) was used to simulate the flow field and pollution transport of the twin-tunnel complementary ventilation system. Fluent software has been applied to solve 3-D continuity, momentum, turbulence kinetic energy, turbulence energy dissipation rate, and pollutant transport equations in steady and incompressible condition. A standard k-ε turbulence model and simple algorithm are used for the model. The governing equations are

$$\nabla \cdot \mathbf{u} = 0 \tag{3}$$

$$\rho \mathbf{u} \cdot \nabla \mathbf{u} - (\mu + \mu_T) \nabla^2 \mathbf{u} = -\nabla p + \rho g \tag{4}$$

$$\rho \mathbf{u} \cdot \nabla k - \nabla \left[\left(\mu + \frac{\mu_T}{\sigma_k} \right) \nabla k \right] = p_k - \rho \varepsilon \tag{5}$$

$$\rho \mathbf{u} \cdot \nabla \varepsilon - \nabla \left[\left(\mu + \frac{\mu_T}{\sigma_\varepsilon} \right) \nabla \varepsilon \right] = \frac{C_1 p_k \varepsilon}{k} - \frac{C_2 p_k \varepsilon^2}{k} \tag{6}$$

$$\rho \mathbf{u} \cdot \nabla \varphi - \Gamma \nabla^2 \varphi = S_\varphi \tag{7}$$

Here $\mathbf{u}$ is Reynolds averaged velocity vector, ρ is the density, μ is the kinetic viscosity, μ_T is the eddy viscosity, g is gravity acceleration, p is pressure, k is turbulence kinetic energy, p_k and ε are the turbulent kinetic energy dissipation rate, φ is the concentration of the pollutant in the domain, S_φ is the pollutant source term, and Γ is the scalar diffusion coefficient. The constants in the model are $C_1 = 1.44$, $C_2 = 1.92$, $C_\mu = 0.09$, $\sigma_\varepsilon = 1.30$, and $\sigma_k = 1.0$. To simplify the model, the amount of particle emitted from vehicle in tunnel was considered as the pollutant source whose distribution is continuous and uniform in tunnel longitudinal direction, which was based on assuming that the rate of particulate matter emitted from vehicle per second is stable and the vehicle passes through the tunnel at constant speed.

3.2. CFD Simulation Model of the Twin-Tunnel Complementary Ventilation System. The tunnel investigated is a twin-tunnel tunnel, the uphill tunnel length is 4910m, and the downhill tunnel length is 4908m. To reduce the element number of model and reduce the computation cost and achieve an accurate solution, the reduced scale numerical simulation model was obtained from the full scale one by means of Euler scaling method, which preserves geometrical, kinematic and dynamic similitude, and similarities of the initial and boundary condition.

In the reduced scale numerical simulation model, the shape was similarity to the full scale model, the cross-sectional scaling ratio of 1/1 (8), and thus the length-scaling ratio of section 2 and section 5 is also 1/1 (9), but the length-scaling ratio of section 1, section 3, section 4, and section 6 is 1/6 (10) to reduce the length of the numerical simulation model and reduce the element number, because the airflow velocity field is uniform distributed in the longitudinal direction in these sections.

$$\frac{D_f}{D_m} = 1 \tag{8}$$

$$\frac{L_{f2}}{L_{m2}} = \frac{L_{f5}}{L_{m5}} = 1 \tag{9}$$

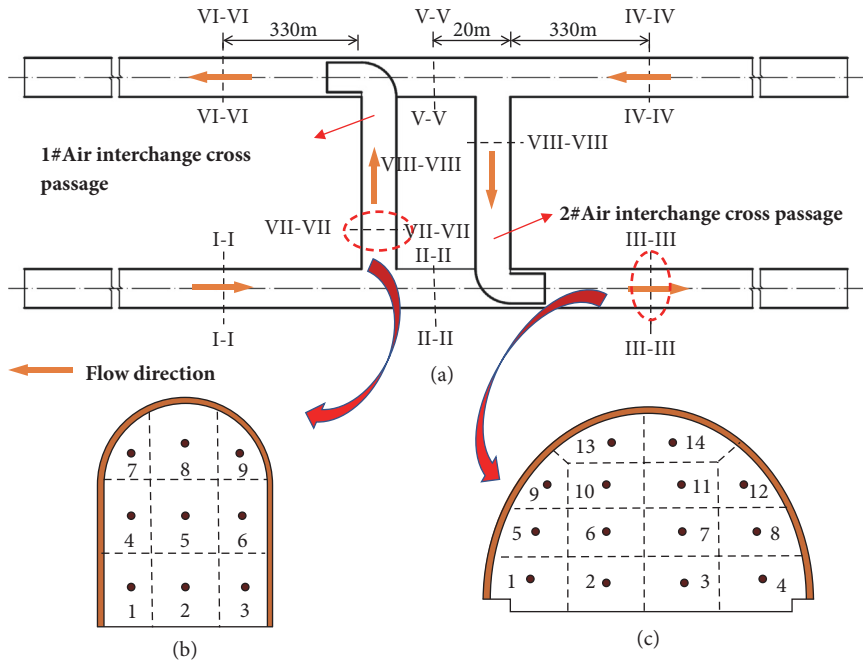

Figure 3: Field measurement scheme: (a) the location of monitored cross-sections, (b) detail of the cross-sections VII-VII and VIII-VIII, and (c) detail of the cross-sections I-I, II-II, III-III, IV-IV, V-V, and VI-VI.

Figure 4: Field measurement: (a) testing preparation in 2# air interchange cross-passage and (b) testing progress in tunnel.

$$\frac{L_{f1}}{L_{m1}} = \frac{L_{f3}}{L_{m3}} = \frac{L_{f4}}{L_{m4}} = \frac{L_{f6}}{L_{m6}} = 6 \tag{10}$$

where L is the length, D is the equivalent diameter, and the subscripts f and m indicate the full scale tunnel and reduced scale numerical simulation model of tunnel, respectively.

Euler scaling method is based on the Euler number preservation and the Euler number is defined as

$$Eu = \frac{\Delta p}{(1/2)\,\rho v^2} \tag{11}$$

where Δp is the pressure losses due to boundary layer resistance of the sections in the tunnel.

During the process of researching fluid motion, fluid flow of both the reduced scale numerical simulation model and full scale model must be kinematical similarity and dynamic similarity; thus, the velocity of each section in the reduced scale numerical simulation model should be as same as them in the full scale model and the velocity is scaled as

$$\frac{v_{fi}}{v_{mi}} = 1 \tag{12}$$

According to Euler scaling method, in which the Euler number of each section in full scale model and the Euler number of the corresponding section in reduced scale numerical simulation model are equal, the scaling factor for the pressure losses can be calculated as

$$\frac{\Delta p_{fi}}{(1/2)\,\rho {v_{fi}}^2} = \frac{\Delta p_{mi}}{(1/2)\,\rho {v_{mi}}^2} \tag{13}$$

from which the pressure loss scaling factor is

$$\frac{\Delta p_{fi}}{\Delta p_{mi}} = 1 \tag{14}$$

where Δp_{fi} is the pressure losses of each section in full scale model and Δp_{mi} is the pressure losses of the corresponding section in reduced scale numerical simulation model, which can be obtained by the following expression:

$$\Delta p_{fi} = \frac{1}{2}\rho {v_{fi}}^2 \cdot \lambda_{fi} \cdot \frac{L_{fi}}{D_f} \tag{15}$$

$$\Delta p_{mi} = \frac{1}{2}\rho {v_{mi}}^2 \cdot \lambda_{mi} \cdot \frac{L_{mi}}{D_m} \tag{16}$$

where λ_{fi} is friction loss factors of sections in full scale model and the λ_{mi} is equivalent friction loss factions of sections in reduced scale numerical simulation model.

Introducing (10), (15), and (16) into (14), then the final function relation among the equivalent friction loss factors of reduced scale numerical simulation model (λ_{mi}) and friction loss factors of full scale model (λ_{fi}) in section 1, section 3, section 4, and section 6 is as follows:

$$\frac{\lambda_{f1}}{\lambda_{m1}} = \frac{\lambda_{f3}}{\lambda_{m3}} = \frac{\lambda_{f4}}{\lambda_{m4}} = \frac{\lambda_{f6}}{\lambda_{m6}} = \frac{L_{m1}}{L_{f1}} = \frac{L_{m3}}{L_{f3}} = \frac{L_{m4}}{L_{f4}} = \frac{L_{m6}}{L_{f6}} = \frac{1}{6} \tag{17}$$

Introducing (9), (15), and (16) into (14), then the final function relation among the equivalent friction loss factors of reduced scale numerical simulation model (λ_{mi}) and friction loss factors of full scale model (λ_{fi}) in section 2, section 5 is as follows:

$$\frac{\lambda_{f2}}{\lambda_{m2}} = \frac{\lambda_{f5}}{\lambda_{m5}} = \frac{L_{f2}}{L_{m2}} = \frac{L_{f5}}{L_{m5}} = 1 \tag{18}$$

According to "Guidelines for Design of Ventilation of Highway Tunnels" (2014) [72], the friction loss faction of tunnel $\lambda_{fi} = 0.02$, so the equivalent friction loss factions of section 1, section3, section 4, and section 6 in the reduced scale numerical simulation model are 6 times the friction loss factions in full scales model, respectively, and the equivalent friction loss factions of section 2 and section5 in the reduced scale numerical simulation model are as same as the friction loss factions in the full scales model, respectively, which is shown as follows:

$$\begin{aligned} \lambda_{m1} = \lambda_{m3} = \lambda_{m4} = \lambda_{m6} = 0.12 \\ \lambda_{m2} = \lambda_{m5} = 0.02 \end{aligned} \tag{19}$$

In the reduced scale numerical simulation model investigated, the equivalent friction loss factions λ_{mi} (i = 1, 2, 3, 4, 5, 6) should satisfy (19), in order to preserve the flow in which each section was similar to the flow in corresponding section in the full scale tunnel, respectively. Based on this method, the different scaling ratios did not affect the simulation results.

The reduced scale of twin-tunnel complementary ventilation system to be modeled consists of twin parallel tunnels with the length 900m including 100m section 2 and 100 m section 5, width 12m and height 8m, and the connecting transverse ducts with the width 5 m and height 6.35 m. For grid

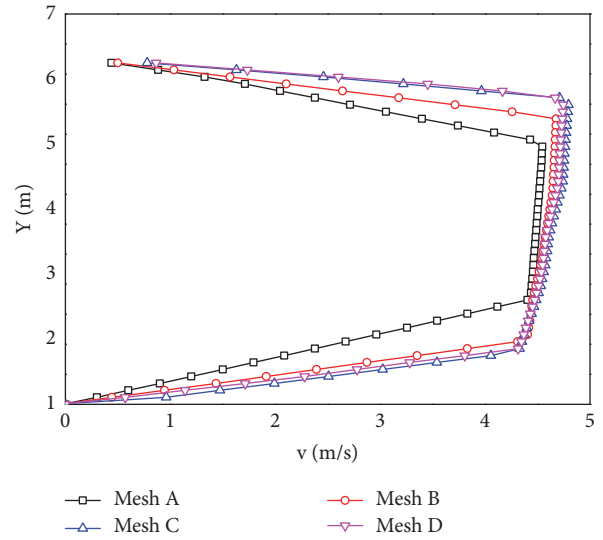

Figure 5: Mesh analysis.

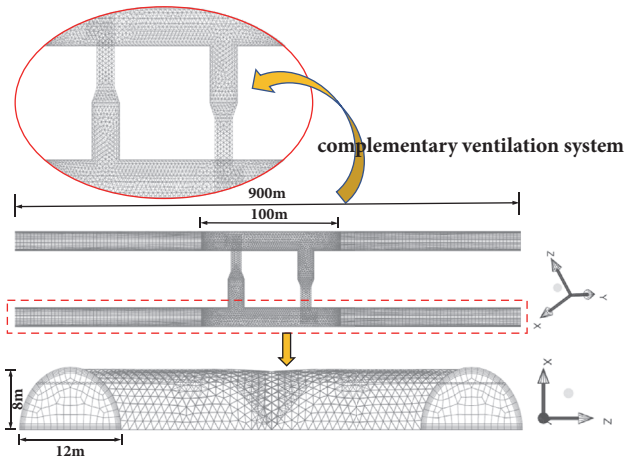

Figure 6: Geometry and meshing of the numerical model.

generation process, a multizone grid approach was applied. Structured mesh was used over the entire computational domain except for air interchange cross-passage zones. Unstructured mesh was applied for air interchange cross-passage zones. Independence mesh tests were carried out with four different mesh sizes to achieve optimal grid for the computational domain. The mesh sizes analyzed were shown in Table 1. The mesh analysis carried out the velocity profile along the tunnel center line on the cross-section 50m away from each air interchange passage outlet in the tunnel shown in Figure 5. The velocity profile along the tunnel center line for mesh A has considerable difference from the other two mesh types. Finally mesh C was used for all the simulations in order to achieve acceptable computational time and numerical accuracy. Figure 6 shows the meshing details of the numerical model which has 583586 elements.

3.3. Boundary Condition. The no-slip stationary wall boundary condition was used for solid walls of the tunnel and the connecting ducts, the inlet, and outlet gage pressure

Table 1: Mesh types and sizes.

Mesh	Mesh size in the longitudinal direction(m)	Mesh size on the cross-section of tunnel(m)	Total cells
A	2	1	121937
B	1.5	0.8	296037
C	1	0.5	583586
D	0.5	0.5	813981

Table 2: The levels of factors in number simulation.

Factor	Levers of factor					
	1	2	3	4	5	6
L_{ex}(m)	2400	2880	3120	3360	3600	3840
Q_{ex}(m^3/s)	125	150	175	200	225	250
P_{jet}(Pa)	75	100	125	150	175	—

boundary condition ($P_{inlet} = 0$, $P_{outlet} = 0$) were set for all surrounding open surfaces of inlet block and outlet block. The total amount of particle emission from the vehicles in uphill tunnel is 1.843m^3/s, and the total amount of particle emission from the vehicles in downhill tunnel is 0.442m^3/s. To simulate the airflow in fan located in the tow interchange air cross-passages, a constant velocity was specified on a specific zone located in the air interchange cross-passages. In other words, there is a volume at the middle of air interchange cross-passages whose velocity is fixed so the air is sucked from the fan inlet and exited from the outlet. In this paper, the volume flow rate of the air interchange cross-passage Q_{ex} and distance from tow interchange air cross-passage to uphill tunnel inlet L_{ex} and the jet fan thrust in twin-tunnel P_{jet} are varied to analyze the effect on the characteristic of pollution concentration distribution. In the simulation of different conditions, there are 6 levels of L_{ex} adopted, 2400m, 2880m, 3120m, 3360m, 3600m, and 3840m. There are 6 levels of Q_{ex} and 5 levels of P_{jet}. The levels of factors in number simulation are listed in Table 2.

3.4. Validation. For validation of the computational model, the experimental measurement data of Dabieshan tunnel ventilation system in section 2.1 is used. In the tunnel ventilation, according to (1), the average air velocity v_{ex} by field measurement in 1# air interchange cross-passages and 2# air interchange cross-passages is 2.55 m/s, and the volume flow rate of air interchange cross-passage ($Q_{ex} = v_{ex} \times A_{ex}$) is 87.5$m^3$/s, where A_{ex} is the section area of air interchange passage of 34.5m^2. In the natural ventilation, the natural wind velocity V_m is tested by field measurement and found be 1.9m/s in the uphill tunnel and 2.1m/s in downhill tunnel, and the natural wind pressure is calculated as 25Pa and 35Pa in the uphill tunnel and downhill tunnel, respectively. The particle emitted from the smoke generating compositions has average value of 0.8651m^2/s and 0.7820m^2/s in uphill tunnel and downhill tunnel, respectively. The value is calculated by multiplying the amount of fresh air Q introduced to the tunnel and the average particle concentration C_{av} in

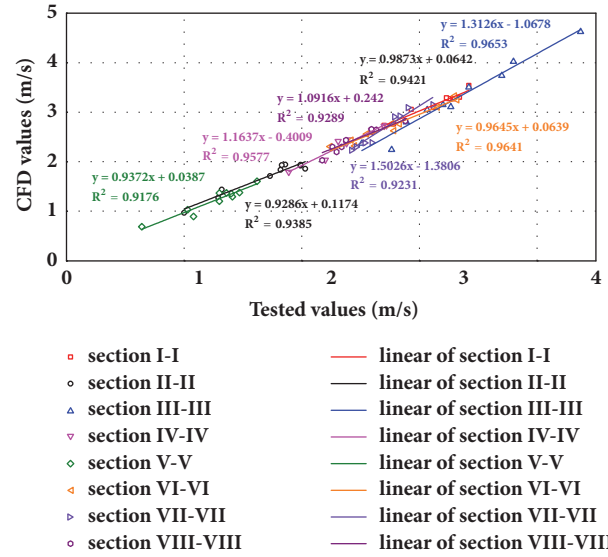

Figure 7: Correlation of average air velocities between CFD value and field measurement.

the cross-section nearing the tunnel exit, in the natural ventilation. Figure 7 shows the correlation of the average air velocity v_i of each part in a cross-section between the CFD model and the field measurement. It can be seen that, in testing sections I-I, III-III, IV-IV, and VI-VI, the air velocities obtained by the CFD model fit the field measurement well and the R^2 coefficients are 0.9556, 0.9743, 0.948, and 0.9616, respectively. In testing sections II-II and V-V, the air flow is affected greatly by the dividing, the air velocity v_i of each part has a wide range of variation, and the R^2 coefficients are 0.9297 and 0.9323. In VII-VII and VIII-VIII, the air flow is affected greatly by the confluence and the turbulence, the air velocities obtained by the CFD model fit the field measurement well and the R^2 coefficients are 0.9231 and 0.9289. Figure 8 shows the correlation of C_{av} of the cross-section between the CFD model and the field measurement. There is a good correlation of C_{av} between the CFD model and field measurement, and the R^2 coefficient is 0.9087.

4. The Numerical Simulation Results and Analysis

4.1. Comparison between the Twin-Tunnel Complementary Ventilation and Longitudinal Ventilation. The performance of the twin-tunnel complementary ventilation and longitudinal ventilation in same traffic condition was investigated. The fresh air introduced to the twin-tunnel by each type of ventilation system is equal, the simulation case is listed in Table 3. Figure 9 shows the result of comparing the particle concentration at horizontal plane (y = 1.5m) for the cases of twin-tunnel complementary ventilation and longitudinal ventilation. For the passengers sitting in their personal cars, the head level is at the height of about 1.5 m above the road. As Figure 9 shows, in the twin-tunnel with longitudinal ventilation, C_U and C_D are 0.00591 and 0.00144, respectively,

Table 3: Simulation case.

Ventilation system	Fresh air volume(m^3/s)		Q_{ex} (m^3/s)	P_{jet} (Pa)	L_{ex} (m)
	Uphill tunnel	Downhill tunnel			
Twin-tunnel complementary ventilation	300	300	200	125	3360
Longitudinal ventilation	300	300	0	169	NO

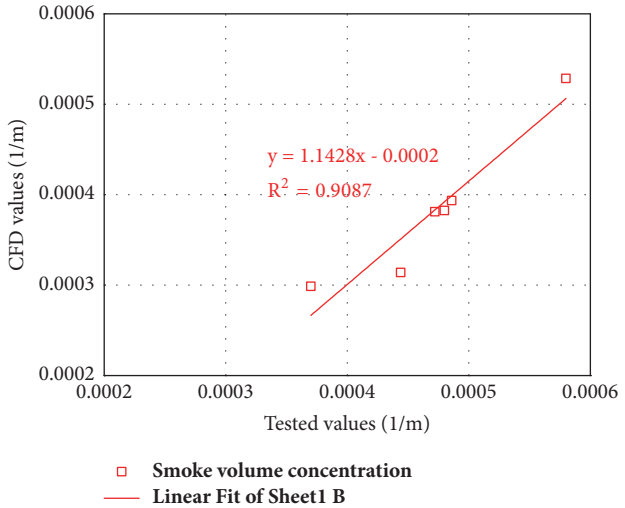

Figure 8: Correlation of average particle concentration between CFD value and field measurement.

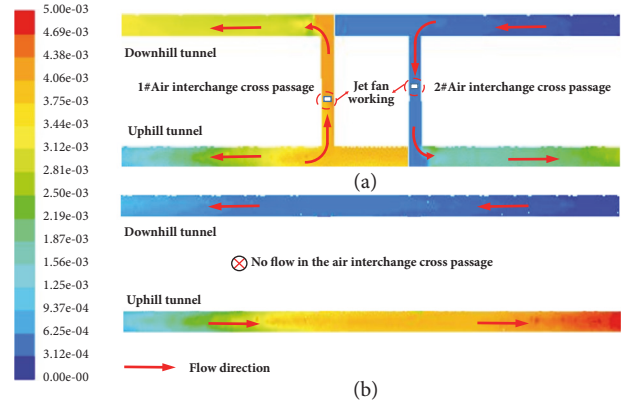

Figure 9: Particle concentration contours (m^{-1}) at horizontal planes y = 1.5m for tunnel with twin-tunnel complementary ventilation, (a) there is flow in air interchange cross-passages, and (b) there is no flow in air interchange cross-passages.

but C_U exceeded the safety limits for particle concentration. In the twin-tunnel with twin-tunnel complementary ventilation, the high concentration pollution air in uphill tunnel passes through 1# air interchange cross-passage into the downhill tunnel, where parts of the pollutants in uphill tunnel were transferred to the downhill tunnel and exhaust through the downhill tunnel outlet and C_D increased to 0.00407 m^{-1}. The low concentration pollution air in downhill tunnel passes through 2# air interchange cross-passage into the uphill tunnel, where parts of the fresh air in downhill tunnel were transferred to the uphill tunnel and dilute pollutant concentration in uphill tunnel and exhaust pass through the uphill tunnel outlet, the C_U reduced to 0.00368 m^{-1}. Thus the twin-tunnel complementary ventilation achieves the effect of adjusting the particle concentration distribution in uphill tunnel and downhill tunnel.

4.2. The Relationship of the Air Interchange Cross-Passages Position and Particle Concentration Profiles. Figure 10 shows that when the interchange air volume is constant, the particle concentration of uphill tunnel outlet C_U is decreased with the increasing of L_{ex}, which is the distance from uphill tunnel inlet to air interchange cross-passage, and the particle concentration of downhill tunnel outlet C_D is increased with the increasing of L_{ex}, and particle concentration ratio of uphill tunnel outlet and downhill tunnel outlet C_U/C_D is decreased following the increasing of L_{ex}; when $C_U/C_D = 1$, the efficiency achieves the best result, and when $C_U/C_D > 1$, the adjusting is excessed. Using Q_{ex} of 200m^3/s and P_{jet} of 125 Pa as examples, when L_{ex} is 2400m, C_U is 0.00472, C_D is 0.00306, and C_U/C_D is 1.54. When L_{ex} is increased to 3840m, C_U is decreased by 33.26%, C_D is increased by 49.34%, and C_U/C_D is decreased by 55.2%. The amount of particles transferred from uphill tunnel to downhill tunnel through 1# air interchange cross-passage increased with the increasing of L_{ex}, which leads to the increase of the amount of particles in downhill tunnel outlet. Meanwhile, the amount of relatively fresh air transferred from downhill tunnel to uphill tunnel through 2# air interchange air cross-passage increased with the increasing of L_{ex}, which leads to decrease of the amount of particles in uphill tunnel outlet; so C_U/C_D is decreased.

To further analyze the relation between C_U/C_D and L_{ex}, when C_U and C_D are same ($C_U/C_D = 1$) (shown as Figure 10(c)), the interchange air volume Q_{ex} is decreased following the increasing of distance L_{ex}. This indicates that the increase of L_{ex} can reduce Q_{ex} in twin-tunnel complementary ventilation design.

4.3. The Relationship of the Interchanged Air Volume and Particle Concentration Profiles. Figure 11 shows that C_U and the C_D are decreased following the increasing of Q_{ex} or P_{jet}. When P_{jet} is constant, C_U/C_D is decreased following the increasing of Q_{ex}; however, when Q_{ex} is constant, C_U/C_D is increased following the increasing of P_{jet}. Section 4.2 discusses the relation between C_U/C_D and L_{ex}. Using L_{ex} of 3360 m and P_{jet} of 175 Pa as example, when the interchange air volume increases from 150 m^3/s to 275 m^3/s, C_U decreases by 26.19%, C_D decreases by 4.34%, and C_U/C_D decreases by 30.5%. Using L_{ex} of 3360m and the fan thrust of 125 Pa as

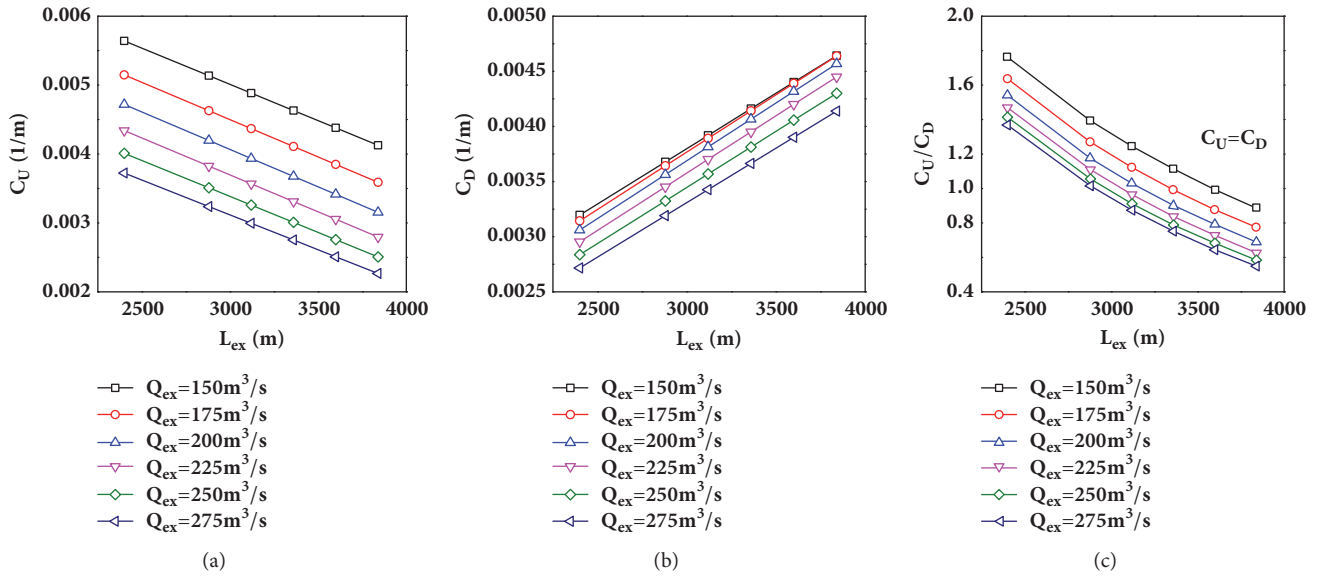

FIGURE 10: Particle concentration profiles variation for various air interchange cross-passages positions: (a) the particle concentration in uphill tunnel outlet, (b) the particle concentration in uphill tunnel outlet, and (c) the particle concentration ratio of uphill tunnel outlet and downhill tunnel outlet.

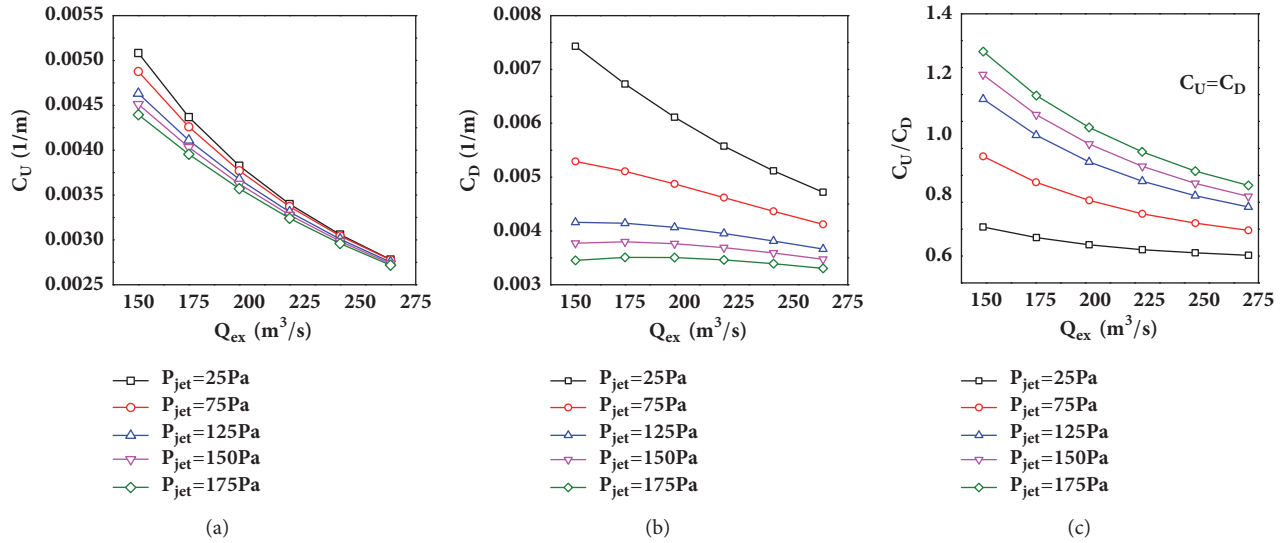

FIGURE 11: Particle concentration profiles variation for various interchanged air volume: (a) the particle concentration in uphill tunnel outlet, (b) the particle concentration in uphill tunnel outlet, and (c) the particle concentration ratio of uphill tunnel outlet and downhill tunnel outlet.

example, when the interchange air volume increases from 150 m^3/s to 275 m^3/s, C_U decreases by 40.6%, C_D decreases by 12%, and C_U/C_D decreased by 32.5%. It can be seen that the influence of Q_{ex} on C_U is greater than that of C_D and the influence degree of Q_{ex} is decreased with the increasing of P_{jet}. On the other hand, using Q_{ex} of 175 m^3/s as example, when the jet fan thrust increases from 25 Pa to 175 Pa, C_U decreases by 9.46%, C_D decreases by 47.85%, and C_U/C_D increases by 73.6%. It can be seen that the influence of P_{jet} on the C_U is less than that of C_D. To further analyze the relation between C_U/C_D and Q_{ex}, when C_U and C_D are the same (C_U/C_D = 1) (shown as Figure 11(c)), the jet fan thrust P_{jet} is increased following the increasing of interchanged air volume Q_{ex}.

4.4. Orthogonal Analysis of the Ventilation Parameters. As discussed above, the parameters, including the distance between uphill tunnel inlet to air interchange cross-passage L_{ex} and the volume flow rate of the air interchange cross-passage Q_{ex} and jet fan thrust P_{jet}, have influence on the efficiency of adjusting the particle concentration distribution in uphill tunnel and downhill tunnel by twin-tunnel complementary ventilation. The orthogonal method experimental

Table 4: Factors and levels of orthogonal experiment.

Factor		Levers of factor				
		1	2	3	4	5
A	Q_{ex}(m^3/s)	150	175	200	225	250
B	L_{ex}(m)	2880	3120	3360	3600	3840
C	P_{jet}(Pa)	75	100	125	150	175

Table 5: Orthogonal table and test results.

	Factor					
NO.	A	D	B	E	C	C_U/C_D
1	175	1	312	1	100	1.045
2	175	2	336	2	125	0.992
3	175	3	360	3	150	0.945
4	175	4	384	4	175	0.902
5	200	1	336	3	175	1.019
6	200	2	312	4	150	1.093
7	200	3	384	1	125	0.690
8	200	4	360	2	100	0.730
9	225	1	360	4	125	0.727
10	225	2	384	3	100	0.579
11	225	3	312	2	175	1.065
12	225	4	336	1	150	0.888
13	250	1	384	2	150	0.622
14	250	2	360	1	175	0.761
15	250	3	336	4	100	0.744
16	250	4	312	3	125	0.913
K_1	3.884	3.413	4.116	3.384	3.098	T = 13.715
K_2	3.532	3.425	3.643	3.409	3.322	Q = 12.164
K_3	3.260	3.444	3.162	3.456	3.548	P = 11.757
K_4	3.040	3.433	2.794	3.466	3.747	
R	0.844	0.031	1.322	0.083	0.649	
SS_j	0.099	0.000	0.248	0.001	0.059	

design is used to explore the influence degree of every factor, and the result is used to optimize the twin-tunnel complementary ventilation system design. Based on consideration of the prototype, four levels for each factor are determined in this study. The factors and levels are shown in Table 4. Considering accuracy of the test and total number of test, an orthogonal table of L_{16} (4^5) is determined for the problem with three factors and four levels for each factor, as shown in Table 5. A, B, and C indicate the factors of Q_{ex}, L_{ex}, and P_{jet}. The vacant columns without factors and interaction are used for error analysis. Observed variables of the test results are simulation results of the efficiency of adjusting the particle concentration distributed in twin-tunnel C_U/C_D of levels of three factors, as shown in Table 5.

The sum of squared deviations caused by each factor SS_j is defined as (20). The total square sum of deviations corresponding to all the vacant columns SS_e is defined as (21) and Q, P, and T are defined as (22)~(24)

$$SS_j = \frac{r}{n}\left(\sum_{i=1}^{r} K_i^2\right) - P \tag{20}$$

$$SS_e = \sum SS_{VacantColumns} \tag{21}$$

$$P = \frac{T^2}{n} \tag{22}$$

$$Q = \sum_{i=1}^{n} y_i^2 \tag{23}$$

$$T = \sum_{i=1}^{n} y_i \tag{24}$$

where n is the number of tests, r is number of levels, y is value of test results, and K_i means the sum of text results at one column when the number of the levers is i.

The degree of freedom corresponding to sum of squared deviations of one column df_j is defined as (25) and the degree of freedom of error df_e is defined as (26). The mean square of a factor MS_j is calculated by (27) and MS_e is calculated by (28) (Table 6). F_j value of factors can be calculated by (29) and the results are shown in Table 7. The greater the difference F value and the corresponding critical value are, the more

Table 6: Values of mean square.

MS_A	MS_D	MS_B	MS_E	MS_C	MS_e
0.033	0.000	0.083	0.000	0.020	0.000

Table 7: Contrast table of significance.

Source of difference	SS_j	df_j	MS_j	F_j	$F_{0.05}$	Significance (relative)
A	0.0994	3	0.0331	155.878	6.39	II
B	0.2480	3	0.0827	389.032	6.39	I
C	0.0590	3	0.0197	92.557	6.39	III
e^{Δ}	0.0013	6	0.0017			
Total	0.4076	15				

significant the influence of the factor on the test results is. When the significance level a is selected as 0.05, the critical value F_α is shown in Table 7. The greater the difference F_j and the corresponding critical value F_α are, the more significant the influence of the factor on the test results is. It can be seen that the important order of three factors having an effect on the C_U/C_D is sequence of the importance is L_{ex}, Q_{ex}, and P_{jet}. Therefore, in the design of the system, the position of air interchange cross-passage is to be considered first; then controlling the interchanged air volume and meeting the fresh air volume required are to be considered. R also indicates influence degree of a factor on the test results. A column with maximum value of R shows that the levels of the factor have the biggest influence on the test results; it is the most important factor. There is a relation of R, which is that $R_B > R_A > R_C$, as shown in Table 4, and the sequence of factors according to their importance is the same as the result of F_j.

$$df_j = r - 1 \tag{25}$$

$$df_e = \sum df_{VavantColumns} \tag{26}$$

$$MS_j = \frac{SS_j}{df_j} \tag{27}$$

$$MS_e = \frac{SS_e}{df_e} \tag{28}$$

$$F_j = \frac{MS_j}{MS_e} \tag{29}$$

5. Conclusions

(1) When L_{ex} is increased, C_U is decreased and C_D increases. Using Q_{ex} of 200m^3/s and P_{jet} of 125 Pa as examples, following L_{ex} being increased from 2400 to 3840m, C_U is decreased by 33.26%, and C_D is increased by 49.34%, while the influence of L_{ex} on C_U is greater than C_D. When C_U and C_D are same ($C_U/C_D = 1$), the efficiency of ventilation system achieves the best result, and the Q_{ex} is decreased following the increasing of L_{ex}.

(2) When Q_{ex} or P_{jet} is increased, C_U and C_D are decreased. Using L_{ex} of 3360m and P_{jet} of 175 Pa as example, when Q_{ex} increases from 150 m^3/s to 275 m^3/s, C_U decreases by 26.19% and C_D decreases by 4.34%, so the influence of Q_{ex} on C_U is greater than C_D. However, using Q_{ex} of 175 m^3/s as example, when P_{jet} increases from 25 Pa to 175 Pa, C_U decreasse by 9.46% and C_D decreases by 47.85%, so the influence of P_{jet} on C_U is less than C_D. When C_U and C_D are the same ($C_U/C_D = 1$), Q_{ex} is increased following the increasing of P_{jet}.

(3)C_U/C_D reflects the efficiency of twin-tunnel complementary ventilation system, and the efficiency increases with C_U/C_D decreasing. According to the orthogonal experiment result, the important order of three factors having an effect on C_U/C_D is sequence of the importance, which is L_{ex}, Q_{ex}, P_{jet}. This means that increasing L_{ex} has most important influence on decreasing C_U/C_D, L_{ex} is considered firstly in ventilation designing, and increasing Q_{ex} also can decrease C_U/C_D, which is considered in the ventilation operation secondly, and P_{jet} is mainly to supply part of the fresh air and guide the air flow in the direction of the tunnel; decreasing P_{jet} has the least important influence on decreasing C_U/C_D.

Data Availability

The data used to support the findings of this study are available from the corresponding author upon request.

Conflicts of Interest

The authors declare that there are no conflicts of interest regarding the publication of this paper.

Acknowledgments

The authors would like to acknowledge the financial support for this work provided by the China Railway Siyuan Survey and Design Group R&D Program (2017k81-1), the Special Fund for Basic Scientific Research of Central Colleges

of Chang'an University (nos. 310821172004, 310821153312, 310821165011, 310821151018, and 310821173312), the Special Fund for Scientific Research Project of Shaanxi Provincial Education Department (2013JK0958), and the Project on Social Development of Shaanxi Provincial Science and Technology Department (nos. 2018SF-382, 2018SF-378).

References

[1] F. Mei, F. Tang, X. Ling, and J. Yu, "Evolution characteristics of fire smoke layer thickness in a mechanical ventilation tunnel with multiple point extraction," *Applied Thermal Engineering*, vol. 111, pp. 248–256, 2017.

[2] M. Juraeva, K. Jin Ryu, S.-H. Jeong, and D. J. Song, "Influence of mechanical ventilation-shaft connecting location on subway tunnel ventilation performance," *Journal of Wind Engineering & Industrial Aerodynamics*, vol. 119, pp. 114–120, 2013.

[3] R. J. De Dear and G. S. Brager, "Thermal comfort in naturally ventilated buildings: Revisions to ASHRAE Standard 55," *Energy and Buildings*, vol. 34, no. 6, pp. 549–561, 2002.

[4] G. M. Stavrakakis, M. K. Koukou, M. G. Vrachopoulos, and N. C. Markatos, "Natural cross-ventilation in buildings: Building-scale experiments, numerical simulation and thermal comfort evaluation," *Energy and Buildings*, vol. 40, no. 9, pp. 1666–1681, 2008.

[5] F. Muhsin, W. F. M. Yusoff, M. F. Mohamed, and A. R. Sapian, "CFD modeling of natural ventilation in a void connected to the living units of multi-storey housing for thermal comfort," *Energy and Buildings*, vol. 144, pp. 1–16, 2017.

[6] S. J. Emmerich and J. W. Axley, "Natural ventilation review and plan for design and analysis tools," National Institute of Standards and Technology NIST IR 6781, 2001.

[7] J. O. P. Cheung and C.-H. Liu, "CFD simulations of natural ventilation behaviour in high-rise buildings in regular and staggered arrangements at various spacings," *Energy and Buildings*, vol. 43, no. 5, pp. 1149–1158, 2011.

[8] G. Gan, "Dynamic interactions between the ground heat exchanger and environments in earth-air tunnel ventilation of buildings," *Energy and Buildings*, vol. 85, pp. 12–22, 2014.

[9] G. Evola and V. Popov, "Computational analysis of wind driven natural ventilation in buildings," *Energy and Buildings*, vol. 38, no. 5, pp. 491–501, 2006.

[10] J. Lai, S. He, J. Qiu et al., "Characteristics of seismic disasters and aseismic measures of tunnels in Wenchuan earthquake," *Environmental Earth Sciences*, vol. 76, no. 2, article 94, 2017.

[11] Jinxing Lai, Sheng Mao, Junling Qiu et al., "Investigation Progresses and Applications of Fractional Derivative Model in Geotechnical Engineering," *Mathematical Problems in Engineering*, vol. 2016, pp. 1–15, 2016.

[12] Jinxing Lai, Junling Qiu, Jianxun Chen, Yaqiong Wang, and Haobo Fan, "Application of Wireless Intelligent Control System for HPS Lamps and LEDs Combined Illumination in Road Tunnel," *Computational Intelligence and Neuroscience*, vol. 2014, Article ID 429657, pp. 1–7, 2014.

[13] J. X. Lai, J. L. Qiu, H. B. Fan, J. X. Chen, and Y. L. Xie, "Freeze-proof method and test verification of a cold region tunnel employing electric heat tracing," *Tunnelling and Underground Space Technology*, vol. 60, pp. 56–65, 2016.

[14] J. Lai, X. Wang, J. Qiu et al., "A state-of-the-art review of sustainable energy based freeze proof technology for cold-region tunnels in China," *Renewable & Sustainable Energy Reviews*, vol. 82, pp. 3554–3569, 2018.

[15] Q. Yan, Y. Xu, W. Zhang, P. Geng, and W. Yang, "Numerical analysis of the cracking and failure behaviors of segmental lining structure of an underwater shield tunnel subjected to a derailed high-speed train impact," *Tunnelling and Underground Space Technology*, vol. 72, pp. 41–54, 2018.

[16] J. L. Qiu, H. Q. Liu, J. X. Lai, H. P. Lai, J. X. Chen, and K. Wang, *Investigating the long term settlement of a tunnel built over improved loessial foundation soil using jet grouting technique , Journal of Performance of Constructed Facilities*, doi, 10.1061/(ASCE)CF.1943-5509, 2018.

[17] J. Qiu, X. Wang, S. He, H. Liu, J. Lai, and L. Wang, "The catastrophic landside in Maoxian County, Sichuan, SW China, on June 24, 2017," *Natural Hazards*, vol. 89, no. 3, pp. 1485–1493, 2017.

[18] J. Qiu, Y. Xie, H. Fan, Z. Wang, and Y. Zhang, "Centrifuge modelling of twin-tunnelling induced ground movements in loess strata," *Arabian Journal of Geosciences*, vol. 10, no. 22, 2017.

[19] W. Zhou, H. Qin, J. Qiu et al., "Building information modelling review with potential applications in tunnel engineering of China," *Royal Society Open Science*, vol. 4, no. 8, 2017.

[20] Q. Yan, L. Song, H. Chen, W. Chen, S. Ma, and W. Yang, "Dynamic Response of Segment Lining of Overlapped Shield Tunnels Under Train-Induced Vibration Loads," *Arabian Journal for Science and Engineering*.

[21] J. Qiu, X. Wang, J. Lai, Q. Zhang, and J. Wang, "Response characteristics and preventions for seismic subsidence of loess in Northwest China," *Natural Hazards*, vol. 92, no. 3, pp. 1909–1935, 2018.

[22] Z. Zhang, X. Shi, B. Wang, and H. Li, "Stability of NATM tunnel faces in soft surrounding rocks," *Computers & Geosciences*, vol. 96, pp. 90–102, 2018.

[23] Z. F. Wang, S. L. Shen, W. C. Cheng et al., "Simple Method to Predict Ground Displacements Caused by Installing Horizontal Jet-Grouting Columns," *Mathematical Problems in Engineering*, vol. 2018, pp. 1–11, 2018.

[24] Z. F. Wang, Y. Q. Wang, and W. C. Cheng, *Investigation into Geohazards during Urbanization Process of Xi'an, China*, vol. 92, no. 3, pp. 1937–1953, 2018.

[25] X. Li, C. Qi, and Z. Shao, "A microcrack growth-based constitutive model for evaluating transient shear properties during brittle creep of rocks," *Engineering Fracture Mechanics*, vol. 194, pp. 9–23, 2018.

[26] Q. X. Yan, H. Chen, W. Y. Chen, J. C. Zhang, and X. Huang, "Dynamic Characteristic and Fatigue Accumulative Damage of a Cross Shield Tunnel Structure under Vibration Load," *Shock and vibration*, vol. 2018, 14 pages, 2018.

[27] Q. X. Yan, B. J. Li, Z. X. Deng, and B. Li, "Dynamic responses of shield tunnel structures with and without secondary lining upon impact by a derailed train," *Structural Engineering and Mechanics*, vol. 65, pp. 741–750, 2018.

[28] H. Yu, Y. Yuan, G. Xu, Q. Su, X. Yan, and C. Li, "Multi-point shaking table test for long tunnels subjected to non-uniform seismic loadings - part II: Application to the HZM immersed tunnel," *Soil Dynamics and Earthquake Engineering*, vol. 108, pp. 187–195, 2018.

[29] Y. Luo, J. Chen, S. Gao, X. Deng, and P. Diao, "Stability analysis of super-large-section tunnel in loess ground considering water infiltration caused by irrigation," *Environmental Earth Sciences*, vol. 76, no. 22, 2017.

[30] H. Yu, X. Yan, A. Bobet, Y. Yuan, G. Xu, and Q. Su, "Multi-point shaking table test of a long tunnel subjected to non-uniform seismic loadings," *Bulletin of Earthquake Engineering*, vol. 16, no. 2, pp. 1041–1059, 2018.

[31] F. Tang, Z. L. Cao, Q. Chen, N. Meng, Q. Wang, and C. G. Fan, "Effect of blockage-heat source distance on maximum temperature of buoyancy-induced smoke flow beneath ceiling in a longitudinal ventilated tunnel," *International Journal of Heat and Mass Transfer*, vol. 109, pp. 683–688, 2017.

[32] S. Takeuchi, T. Aoki, F. Tanaka, and K. A. M. Moinuddin, "Modeling for predicting the temperature distribution of smoke during a fire in an underground road tunnel with vertical shafts," *Fire Safety Journal*, vol. 91, pp. 312–319, 2017.

[33] H. Cong, X. Wang, P. Zhu, T. Jiang, and X. Shi, "Experimental study of the influences of board size and position on smoke extraction efficiency by natural ventilation through a board-coupled shaft during tunnel fires," *Applied Thermal Engineering*, vol. 128, pp. 614–624, 2018.

[34] T. Du, D. Yang, S. Peng, Y. Liu, and Y. Xiao, "Performance evaluation of longitudinal and transverse ventilation for thermal and smoke control in a looped urban traffic link tunnel," *Applied Thermal Engineering*, vol. 96, pp. 490–500, 2016.

[35] Q. Liang, Y. Li, J. Li, H. Xu, and K. Li, "Numerical studies on the smoke control by water mist screens with transverse ventilation in tunnel fires," *Tunnelling and Underground Space Technology*, vol. 64, pp. 177–183, 2017.

[36] B. Lou, Y. Qiu, and X. Long, "Maximum Smoke Temperature in Non-Smoke Model Evacuation Region for Semi-Transverse Tunnel Fire," *Journal of Applied Fluid Mechanics*, vol. 10, no. 4, pp. 1139–1151, 2017.

[37] R. Ballesteros-Tajadura, C. Santolaria-Morros, and E. Blanco-Marigorta, "Influence of the slope in the ventilation semi-transversal system of an urban tunnel," *Tunnelling and Underground Space Technology*, vol. 21, no. 1, pp. 21–28, 2006.

[38] Y. Wu and M. Z. A. Bakar, "Control of smoke flow in tunnel fires using longitudinal ventilation systems—a study of the critical velocity," *Fire Safety Journal*, vol. 35, no. 4, pp. 363–390, 2000.

[39] S. Bogdan, B. Birgmajer, and Z. Kovačić, "Model predictive and fuzzy control of a road tunnel ventilation system," *Transportation Research Part C: Emerging Technologies*, vol. 16, no. 5, pp. 574–592, 2008.

[40] F. Wang, M. Wang, S. He, J. Zhang, and Y. Deng, "Computational study of effects of jet fans on the ventilation of a highway curved tunnel," *Tunnelling and Underground Space Technology*, vol. 25, no. 4, pp. 382–390, 2010.

[41] F. Wang, M. Wang, and Q. Wang, "Numerical study of effects of deflected angles of jet fans on the normal ventilation in a curved tunnel," *Tunnelling and Underground Space Technology*, vol. 31, pp. 80–85, 2012.

[42] E. Eftekharian, A. Dastan, O. Abouali, J. Meigolinedjad, and G. Ahmadi, "A numerical investigation into the performance of two types of jet fans in ventilation of an urban tunnel under traffic jam condition," *Tunnelling and Underground Space Technology*, vol. 44, pp. 56–67, 2014.

[43] M. Musto and G. Rotondo, "Numerical comparison of performance between traditional and alternative jet fans in tiled tunnel in emergency ventilation," *Tunnelling and Underground Space Technology*, vol. 42, pp. 52–58, 2014.

[44] A. Kazemipour, H. Afshin, and B. Farhanieh, "Numerical–Analytical Assessment of Fire and Ventilation Interaction in Longitudinally Ventilated Tunnels Using Jet Fans," *Heat Transfer Engineering*, vol. 38, no. 5, pp. 523–537, 2017.

[45] S. R. Lee and H. S. Ryou, "A numerical study on smoke movement in longitudinal ventilation tunnel fires for different aspect ratio," *Building and Environment*, vol. 41, no. 6, pp. 719–725, 2006.

[46] F. Tang, L. J. Li, F. Z. Mei, and M. S. Dong, "Thermal smoke back-layering flow length with ceiling extraction at upstream side of fire source in a longitudinal ventilated tunnel," *Applied Thermal Engineering*, vol. 106, pp. 125–130, 2016.

[47] F. Tang, F. Z. Mei, Q. Wang, Z. He, C. G. Fan, and C. F. Tao, "Maximum temperature beneath the ceiling in tunnel fires with combination of ceiling mechanical smoke extraction and longitudinal ventilation," *Tunnelling and Underground Space Technology*, vol. 68, pp. 231–237, 2017.

[48] T. Chen, Y. Lee, and C. Hsu, "Investigations of piston-effect and jet fan-effect in model vehicle tunnels," *Journal of Wind Engineering & Industrial Aerodynamics*, vol. 73, no. 2, pp. 99–110, 1998.

[49] World Road Association, *Road Tunnels: Vehicle Emissions and Air Demand For Ventilation*, PIARC Committee on Road Tunnels Operation (C4), 2012.

[50] C.-Y. Chung and P.-L. Chung, "A numerical and experimental study of pollutant dispersion in a traffic tunnel," *Environmental Modeling & Assessment*, vol. 130, no. 1-3, pp. 289–299, 2007.

[51] S. Bari and J. Naser, "Simulation of airflow and pollution levels caused by severe traffic jam in a road tunnel," *Tunnelling and Underground Space Technology*, vol. 25, no. 1, pp. 70–77, 2010.

[52] Y. Li, Y. Yang, H. Yu, and G. Roberts, "Principal Stress Rotation under Bidirectional Simple Shear Loadings," *KSCE Journal of Civil Engineering*, vol. 22, no. 5, pp. 1651–1660, 2018.

[53] Y. Luo, J. Chen, P. Huang, M. Tang, X. Qiao, and Q. Liu, "Deformation and mechanical model of temporary support sidewall in tunnel cutting partial section," *Tunnelling and Underground Space Technology*, vol. 61, pp. 40–49, 2017.

[54] J.-Y. Kim and K.-Y. Kim, "Effects of vent shaft location on the ventilation performance in a subway tunnel," *Journal of Wind Engineering & Industrial Aerodynamics*, vol. 97, no. 5-6, pp. 174–179, 2009.

[55] C.-J. Lin, Y. K. Chuah, and C.-W. Liu, "A study on underground tunnel ventilation for piston effects influenced by draught relief shaft in subway system," *Applied Thermal Engineering*, vol. 28, no. 5-6, pp. 372–379, 2008.

[56] H. Y. Cong, X. S. Wang, P. Zhu, T. H. Jiang, and X. J. Shi, "Improvement in smoke extraction efficiency by natural ventilation through a board-coupled shaft during tunnel fires," *Applied Thermal Engineering*, vol. 118, pp. 127–137, 2017.

[57] C. G. Fan, J. Ji, Z. H. Gao, J. Y. Han, and J. H. Sun, "Experimental study of air entrainment mode with natural ventilation using shafts in road tunnel fires," *International Journal of Heat and Mass Transfer*, vol. 56, no. 1-2, pp. 750–757, 2013.

[58] M. A. Berner and J. R. Day, "A new concept for ventilation long twin-tube tunnels," in *Proceedings of the Proc.7th International Symposium on the Aerodynamics and Ventilation of Vehicle Tunnels*, vol. 10, pp. 811–820, 1991.

[59] F. Chen, "Smoke propagation in road tunnels," *Applied Mechanics Reviews*, vol. 53, no. 8, pp. 207–218, 2000.

[60] O. Indrehus and P. Vassbotn, "CO and NO2 pollution in a long two-way traffic road tunnel: Investigation of NO2/NOx ratio and modelling of NO2 concentration," *Journal of Environmental Monitoring*, vol. 3, no. 2, pp. 220–225, 2001.

[61] W. K. Chow and M. Y. Chan, "Field measurement on transient carbon monoxide levels in vehicular tunnels," *Building and Environment*, vol. 38, no. 2, pp. 227–236, 2003.

[62] W. X. Wang, W. S. Zhao, L. X. Huang, V. Vimarlund, and Z. W. Wang, "Applications of terrestrial laser scanning for tunnels: a review," *Journal of Traffic and Transportation Engineering (English Edition)*, vol. 1, no. 5, pp. 325–337, 2014.

[63] T. Wang, W. Han, F. Yang, and W. Kong, "Wind-vehicle-bridge coupled vibration analysis based on random traffic flow simulation," *Journal of Traffic and Transportation Engineering (English Edition)*, vol. 1, no. 4, pp. 293–308, 2014.

[64] W. Cheng, J. C. Ni, A. Arulrajah, and H. Huang, "A simple approach for characterising tunnel bore conditions based upon pipe-jacking data," *Tunnelling and Underground Space Technology*, vol. 71, pp. 494–504, 2018.

[65] Y. Luo, J. Chen, Y. Chen, P. Diao, and X. Qiao, "Longitudinal deformation profile of a tunnel in weak rock mass by using the back analysis method," *Tunnelling and Underground Space Technology*, vol. 71, pp. 478–493, 2018.

[66] AIAA, "Guide for the Verification and validation of computational fluid dynamics simulations," AIAA G-077,1998.

[67] X. Luo, L. Niu, and S. Zhang, "An Algorithm for Traffic Flow Prediction Based on Improved SARIMA and GA," *KSCE Journal of Civil Engineering*.

[68] J. Wang, Z. Song, B. Zhao, X. Liu, J. Liu, and J. Lai, "A Study on the Mechanical Behavior and Statistical Damage Constitutive Model of Sandstone," *Arabian Journal for Science and Engineering*.

[69] Y. Wei, S. Liang, W. Guo, and W. Hansen, "Stress prediction in very early-age concrete subject to restraint under varying temperature histories," *Cement and Concrete Composites*, vol. 83, pp. 45–56, 2017.

[70] Jinxing Lai, Junling Qiu, Jianxun Chen, Haobo Fan, and Ke Wang, "New Technology and Experimental Study on Snow-Melting Heated Pavement System in Tunnel Portal," *Advances in Materials Science and Engineering*, vol. 2015, pp. 1–11, 2015.

[71] X. Nie, X. Wei, X. Li, and C. Lu, "Heat treatment and ventilation optimization in a deep mine," *Advances in Civil Engineering*, In press.

[72] "JTG/T D70/2-02-2014," Guidelines for Design of Ventilation of Highway Tunnels, China Communication Press, Beijing, 2014.